Projections of quantum observables onto classical degrees of freedom in mixed quantum/classical simulations: Understanding why linear response fails for the photoexcited hydrated electron

Michael J. Bedard-Hearn, Ross E. Larsen, and Benjamin J. Schwartz*
Department of Chemistry and Biochemistry, UCLA
607 Charles E. Young Dr. East
Los Angeles, CA 90095-1569

We present a general analytic method for understanding how specific motions of a classical bath influence the dynamics of quantum mechanical observables in mixed quantum/classical molecular dynamics simulations. We apply our method and develop expressions for the special case of quantum solvation, allowing us to examine how specific classical solvent motions couple to the equilibrium energy fluctuations and nonequilibrium energy relaxation of a quantum mechanical solute. As a first application of our formalism, we investigate the motions of classical water underlying the equilibrium and nonequilibrium solvent response functions of the hydrated electron; the results allow us to explain why the linear response approximation fails for this system.

One of the principle goals of molecular dynamics (MD) simulations is to understand how specific molecular motions of a bath influence physical processes of interest. In classical MD, Steele theory [1, 2] can be used to calculate the how a specific dynamical variable, A, is changed by individual bath degrees of freedom by projection. Ladanyi and co-workers have used such projections to understand how specific solvent motions affect equilibrium solvation dynamics [2], and we have extended the projections formalism to nonequilibrium solvation dynamics and uncovered a hidden breakdown of linear response (LR) [3]. There has been no analogous analytical tool, however, for understanding how bath degrees of freedom (DOF) affect quantum mechanical observables, including the Hamiltonian. In this Letter, we present a new formalism for projecting dynamical changes of quantum expectation values in mixed quantum/classical (MQC) simulations onto classical molecular motions. Our method allows us to determine how any measurable quantity associated with the interaction of a quantum wave function and a classical bath is affected by specific motions of the bath.

In classical MD simulations, projections are performed by expanding the time derivative of an observable A using the chain rule, $\dot{A} = \sum_i \dot{\mathbf{R}}_i \cdot \nabla_{\mathbf{R}_i} A$, where $\mathbf{R}$ denotes the bath coordinates and the index i runs over all bath DOF. Integration of each term in the sum with respect to time gives A_i, the projection of A onto bath coordinate i [3, 4]. Here, we use a similar approach to project quantum expectation values onto bath coordinates, and after presenting our new formalism, we apply it to one of the best-studied MQC systems, the hydrated electron [5, 6]. Our analysis shows clearly why LR fails to describe the nonequilibrium solvent relaxation following photoexcitation of this prototypical quantum solute.

In MQC simulations, the Hamiltonian of the quantum subsystem is $\hat{H} = \hat{T} + \hat{U} + \hat{V}_p$, where $\hat{T}$ and $\hat{U}$ are the quantum mechanical kinetic and potential energy operators, and where $\hat{V}_p$ is the pseudopotential, which describes the interaction between the quantum and classical subsystems and thus depends on both the classical ($\mathbf{R}$) and quantal ($\mathbf{r}$) DOF. For a given configuration of the classical particles, the quantum subsystem is defined in terms of the adiabatic eigenvectors $|k\rangle$ and eigenvalues E_k of $\hat{H}$, which evolve according to the classical dynamics, and the time-dependent Schrödinger equation (TDSE). The classical subsystem's dynamics are driven in turn by the classical interaction potential and by the Hellmann-Feynman (HF) force, $\mathbf{F}_{i,\mathrm{HF}} = -\langle\psi|\nabla_{\mathbf{R}_i} V_p|\psi\rangle$, which is the force the quantum subsystem with wave function $|\psi\rangle$ exerts on each classical DOF, $\mathbf{R}_i$. Although the above prescription dictates the precise evolution of a MQC system, it does not provide information as to which *specific* classical DOF influence the dynamics of any particular quantum observable.

To obtain such information, our goal, is to emulate classical Steele theory, and write the time derivative of an observable, in this case a quantum expectation value, in terms of classical gradients. Consider a quantum Hermitian operator $\hat{\Omega}$ and its expectation value with the k^{th} adiabatic state, $\langle\hat{\Omega}\rangle = \langle k|\hat{\Omega}|k\rangle \equiv \Omega_{kk}$. Using the chain rule,

$$\frac{d}{dt}\langle k|\hat{\Omega}|k\rangle = \langle\dot{k}|\hat{\Omega}|k\rangle + \langle k|\hat{\Omega}|\dot{k}\rangle + \langle k|\dot{\hat{\Omega}}|k\rangle. \qquad (1)$$

By inserting a complete set of states into each of the first two terms on the right-hand side of Eq. 1 and introducing the nonadiabatic coupling vectors, $\langle m|\dot{k}\rangle = \sum_i \dot{\mathbf{R}}_i \cdot \langle m|\nabla_{\mathbf{R}_i} k\rangle \equiv \sum_i \dot{\mathbf{R}}_i \cdot \mathbf{d}^i_{mk}$, we obtain

$$\dot{\Omega}_{kk} = \sum_i \Bigg[2\sum_m \dot{\mathbf{R}}_i \cdot \mathbf{d}^i_{km}\Omega_{mk} + \dot{\mathbf{R}}_i \cdot \langle k|\big(\nabla_{\mathbf{R}_i}\hat{\Omega}\big)|k\rangle \Bigg] \equiv \sum_i \dot{\Omega}^i_{kk}, \qquad (2)$$

where m and k index the adiabatic eigenstates of $\hat{H}$, $\Omega_{mk} \equiv \langle m|\hat{\Omega}|k\rangle$, and the sum on i is over each classical DOF. Although the sum on m formally runs over all of the adiabatic states, it likely can be truncated to just a few terms in most practical applications [7]. Thus, Eq. 2 shows that projections of Ω_{kk} onto specific classical coordinates can be obtained by seeing how the velocities of relevant classical DOF alter the adiabatic eigenstates, which in turn alter the quantum expectation value.

Equation 2 is valid for an expectation value associated with a single adiabatic state, but in nonadiabatic MQC simulations, the quantum subsystem is often described as a superposition of the adiabatic eigenvectors, $|\psi\rangle = \sum_k a_k|k\rangle$, which we refer to as a mean field (MF) state. For quantum observables associated with MF states, the projections proceed in a similar manner as for adiabatic states, but for the MF case, the evolution of the density matrix, $\rho_{kk'} = a_k^* a_{k'}$, leads to an unusual cancellation of terms. Using the TDSE,

$$\dot{\rho}_{kk'} = \sum_{m,i} \dot{\mathbf{R}}_i \cdot \left(\rho_{mk'}\mathbf{d}^i_{mk} - \rho_{km}\mathbf{d}^i_{k'm}\right) + \frac{i}{\hbar}\rho_{kk'}E_{kk'}, \quad (3)$$

where $E_{kk'} = E_k - E_{k'}$, we see that

$$\begin{aligned}\frac{d}{dt}\langle\psi|\hat{\Omega}|\psi\rangle = \frac{d}{dt}\langle\hat{\Omega}\rangle &= \frac{i}{\hbar}\sum_{k,k'}\rho_{kk'}\Omega_{kk'}E_{kk'} \\ &\quad + \sum_i \dot{\mathbf{R}}_i \cdot \langle\psi|\nabla_{\mathbf{R}_i}\hat{\Omega}|\psi\rangle \\ &\equiv \frac{i}{\hbar}\sum_{k,k'}\rho_{kk'}\Omega_{kk'}E_{kk'} + \sum_i \dot{\Omega}^i_{\mathrm{MF}} \end{aligned} \quad (4)$$

where the nonadiabatic coupling terms from the derivatives of the eigenvectors exactly cancel with identical terms from the derivative of the density matrix in Eq. 3. The first term in the final expression of Eq. 4 arises from the evolution of the quantum phase in the TDSE; it has no explicit dependence on the classical particles' motions and it vanishes if either $\hat{\Omega}$ is diagonal in the chosen basis or if the density matrix is diagonal. In addition, if $\hat{\Omega}$ has no explicit $\mathbf{R}$ dependence, the second term in the final expression of Eq. 4 also vanishes, so there appears to be no expression analogous to Eq. 2 that determines how the bath DOF influence expectation values associated with quantum superposition states. If $\hat{\Omega}$ does have explicit $\mathbf{R}$ dependence, however, then the second term in Eq. 4 provides the desired information. For either Eq. 2 or Eq. 4, the projection of $\langle\hat{\Omega}\rangle$ onto a classical coordinate i is found by integrating either $\dot{\Omega}^i_{kk}$ or $\dot{\Omega}^i_{\mathrm{MF}}$ with respect to time,

$$\Omega^i(t) - \Omega^i(0) = \int_0^t dt' \dot{\Omega}^i(t'). \quad (5)$$

Thus, Eqs. 2, 4 and 5 allow us to project the dynamics of quantum solutes, even those described by superposition wave functions, onto specific motions of a classical bath.

To illustrate the application of our formalism in MQC simulations, we consider the case of dynamic solvation, in which the classical solvent causes the energy of the quantum solute to relax following excitation. The nonequilibrium relaxation dynamics are described by the solvent response function,

$$S(t) = \frac{\overline{\Delta E}(t) - \overline{\Delta E}(\infty)}{\overline{\Delta E}(0) - \overline{\Delta E}(\infty)}, \quad (6)$$

where the overbar denotes a nonequilibrium ensemble average and $\Delta E = \langle\psi|\hat{H}|\psi\rangle - \langle 0|\hat{H}|0\rangle$ is the energy gap between the excited ($|\psi\rangle$) and ground ($|0\rangle$) states of the quantum solute. In the limit of LR, the nonequilibrium response function is equal to the equilibrium solvation correlation function,

$$C(t) = \langle\delta\Delta E(t)\cdot\delta\Delta E(0)\rangle / \langle(\delta\Delta E)^2\rangle \quad (7)$$

where the fluctuations from the average energy gap [8] are $\delta\Delta E(t) = \Delta E(t) - \langle\Delta E\rangle$, and the angled brackets denote an equilibrium ensemble average. (We note that although LR implies that $S(t) \sim C(t)$, the converse is not necessarily true [3].)

To project the nonequilibrium and equilibrium solvation dynamics onto the motions of classical particles, we take the first time derivative, $J(t) \equiv \dot{S}(t)$, of Eq. 6,

$$J(t) = \sum_i \overline{\Delta\dot{E}_i}(t) / (\overline{\Delta E}(0) - \overline{\Delta E}(\infty)) \equiv \sum_i J_i(t), \quad (8)$$

and the second derivative, $G(t) \equiv -\ddot{C}(t)$, of Eq. 7,

$$G(t) = \sum_{i,j} \frac{\langle\Delta\dot{E}_i(t)\cdot\Delta\dot{E}_j(0)\rangle}{\langle(\delta\Delta E)^2\rangle} \equiv \sum_{i,j} G_{ij}(t). \quad (9)$$

By integrating each projected $J_i(t)$ once and each $G_{ij}(t)$ twice with respect to time, we obtain the desired nonequilibrium and equilibrium projections, $S_i(t)$ and $C_{ij}(t)$, respectively. Since both Eqs. 8 and 9 have $\hat{\Omega} = \hat{H}$, the desired projections from Eqs. 2 and 4 are

$$\begin{aligned}\frac{d}{dt}\langle k|\hat{H}|k\rangle &= \sum_i \dot{\mathbf{R}}_i \cdot \mathbf{F}^i_k = \sum_i \dot{E}^i_k \\ \frac{d}{dt}\langle\psi|\hat{H}|\psi\rangle &= \sum_i \dot{\mathbf{R}}_i \cdot \mathbf{F}^i_{\mathrm{HF}} = \sum_i \dot{E}^i_{\mathrm{MF}}, \end{aligned} \quad (10)$$

where $\cdot\mathbf{F}^i_k = \langle k|\nabla_{\mathbf{R}_i}V_p|k\rangle$ is the adiabatic HF force, and the Cartesian velocities $\dot{\mathbf{R}}_i$ can easily be converted into relative solute-solvent coordinates via unitary transformations. For example, the center-of-mass (com) velocity of each classical particle can be separated into a longitudinal translation (directly toward or away from the quantum solute's center of mass along $\mathbf{n} = \mathbf{R}_{com} - \langle\psi|\hat{r}|\psi\rangle$) and two lateral translations orthogonal to $\mathbf{n}$. Equa-

tions 8–10 provide everything needed to quantify exactly how specific classical solvent motions such as translations or rotations affect the solvation dynamics of quantum solutes.

We now apply these new tools to explore the molecular basis of the solvent relaxation following photoexcitation of the hydrated electron (e^-_{hyd}). The details of our MQC simulations are given elsewhere [9]; briefly, the system contains 200 classical SPC-Flex water molecules [10] and a single excess quantum electron that interacts with the solvent using the Schnitker-Rossky pseudopotential [11]. The velocity Verlet algorithm was used to propagate the classical dynamics with a time-step of 1 fs for the adiabatic, equilibrium trajectories and 0.125 fs for the nonadiabatic, nonequilibrium trajectories. The nonadiabatic runs were calculated using the mean-field with stochastic decoherence (MF-SD) algorithm [12] with $w = 4\ a_0$ for the MF-SD nonadiabatic coupling width; see Ref. [9] for details. Statistics were collected from two uncorrelated 50-ps ground state equilibrium trajectories with the hydrated electron in the ground state and from 50 nonadiabatic, nonequilibrium trajectories started from 25 uncorrelated initial configurations (with the initial velocities reversed to obtain a second run per starting configuration). For each nonequilibrium trajectory, the equilibrated ground-state e^-_{hyd} was promoted to an adiabatic excited state 2.27 ± 0.01 eV above the ground state, near the peak of the calculated e^-_{hyd} absorption spectrum [5]. When calculating nonequilibrium averages, we removed trajectories from the ensemble once they had nonadiabatically relaxed to the ground state; thus, our nonequilibrium ensemble has 50 members at the earliest times, but only 18 members at 600 fs [9].

We note that in most nonadiabatic MD algorithms, including MF-SD, the electronic density matrix undergoes discontinuities whenever the quantum subsystem decoheres [12]. Most MQC MD algorithms partition the changes in the quantum energy among the classical coordinates by scaling the classical momenta along the direction of the nonadiabatic coupling vectors; projections of these rare discontinuous events onto the bath DOF have been discussed elsewhere [13]. For a detailed discussion of how the e^-_{hyd} responds to such events in our simulations, see EPAPS Document No. (number) [14].

Previous calculations by Schwartz and Rossky [5] found that $S(t)$ is similar to $C(t)$ for the excited e^-_{hyd}, suggesting that LR holds for this system. The result is surprising, given more recent studies of classical solvation, which showed that when solutes change size or shape, LR typically does not apply [15]. Since the hydrated electron undergoes both shape and symmetry changes upon excitation (from an *s*-like to a *p*-like wave function), we expect $S(t)$ and $C(t)$ to be very different, or at least that the underlying dynamics coupling to the solvation processes are different. We have revisited the solvation dynamics of this system, and Fig. 1A shows that $S(t)$ and $C(t)$ are in fact completely different, even at the earliest times when the LR approximation is expected to be most applicable. The difference between our results and those in Ref. [5] likely results from poor statistical sampling in Ref. [5], where only 20 nonequilibrium trajectories were used instead of the 50 used here, although the different nonadiabatic MQC algorithms used here and in Ref. [5] may also play a role.

To understand the breakdown of LR for the e^-_{hyd} evident in Fig. 1A, we calculated time-integrated projections of both the nonequilibrium (Fig. 1A, Eq. 8) and equilibrium (Fig. 1B, Eq. 9) solvent response functions onto various classical DOF; details concerning the numerical integration and normalization of the projections are discussed in EPAPS Document No. (number) [14]. Figure 1 shows the projections of the solvent response functions onto water center-of-mass (com) translations, $S_{\rm trans}$ and $C_{\rm trans}$, as well as the longitudinal component of the water com translations (discussed above), $S_{\rm long}$ and $C_{\rm long}$. The figure also shows the sum of the projections onto all the rotational and vibrational DOF, taken as the difference between the total solvent response and the total com translational projection, *e.g.*, $S_{\rm r\text{-}v} = S_{\rm tot} - S_{\rm trans}$; we note that $C_{\rm r\text{-}v}$ also contains cross terms that do not appear in the nonequilibrium projections [2, 3].

The water molecules in our simulations are flexible, so there is no strict way to separately project their vibrational and rotational motions. As a result, we separated the contributions of rotational and vibrational modes using Fourier analysis of $S_{\rm r\text{-}v}(t)$ and $C_{\rm r\text{-}v}(t)$, as shown in EPAPS Document No. (number) [14]. The librational modes of SPC Flex water have frequencies less than $\sim$1000 cm^{-1} and are spectrally well-separated from the vibrational modes, whose frequencies lie between $\sim$1700 and $\sim$4000 cm^{-1}. We found that librations dominate both projected solvent response functions and that vibrational coupling is negligible. Thus, the $S_{\rm r\text{-}v}$ and $C_{\rm r\text{-}v}$ curves plotted in Fig. 1 represent essentially pure librational projections of $S(t)$ and $C(t)$. It is worth noting that a spectral density analysis of the *total* $S(t)$ and $C(t)$ cannot distinguish contributions from translational or librational DOF, or separate the translation-rotation coupling in $C_{\rm r\text{-}v}$, since water translations and librations have overlapping frequency ranges. Our new formalism, however, allows us to cleanly isolate the role of each classical degree of freedom in the nonequilibrium solvent relaxation, $S(t)$, as well as all of the cross-terms in the equilibrium solvent response, $C(t)$.

The projections of $S(t)$ and $C(t)$ make it easy to see that the classical motions underlying the equilibrium and nonequilibrium solvent relaxation of the e^-_{hyd} are quite different. Figure 1B shows that solvent librations and translations contribute equally to the equilibrium solvation correlation function, whereas Fig. 1A indicates that librational motions dominate the nonequilibrium solvent relaxation. Both at and away from equilibrium, trans-

lational solvent motions occur on a single time scale, with longitudinal motions comprising ∼90% of the total translational response. The librational responses, however, are quite different at and away from equilibrium. The equilibrium librational response, $C_{\text{r-v}}$, occurs on two distinct time-scales and is characterized by a rapid inertial relaxation that accounts for ∼1/3 of the total solvation followed by a slower component that is not complete until $t >$∼500 fs. In contrast, the nonequilibrium librational response, $S_{\text{r-v}}$, is extremely rapid; it is nearly complete within ∼50 fs and plays only a minor role in the total nonequilibrium relaxation after 100 fs. Thus, our projection analysis demonstrates that not only do different solvent motions contribute to relaxation with different amplitudes at and away from equilibrium, but that the equilibrium and nonequilibrium solvent dynamics are composed of entirely different types of solvent motions; the large size and shape change that the e^-_{hyd} undergoes upon excitation alters the solute-solvent coupling, leading to a breakdown of LR [15].

In summary, we have presented a new formalism for projecting how classical motions affect quantum observables in MQC MD simulations. Our method can be applied to any quantum operator and provides precise, molecular detail about the coupling between quantum solutes and classical motions. We applied our method to study the solvent relaxation of the prototypical MQC system, the photoexcited e^-_{hyd}, and found that entirely different solvent motions were responsible for the equilibrium and nonequilibrium solvent relaxation, explaining the breakdown of LR for this system. In the future, we plan to use our new formalism to study how quantum-mechanical spins, electron or proton transfer reactions, and quantum mechanical tunneling rates are modulated by specific bath DOF.

Acknowledgements This work was supported by the NSF under grant CHE-0204776. B.J.S. is a Camille-Dreyfus Teacher-Scholar.

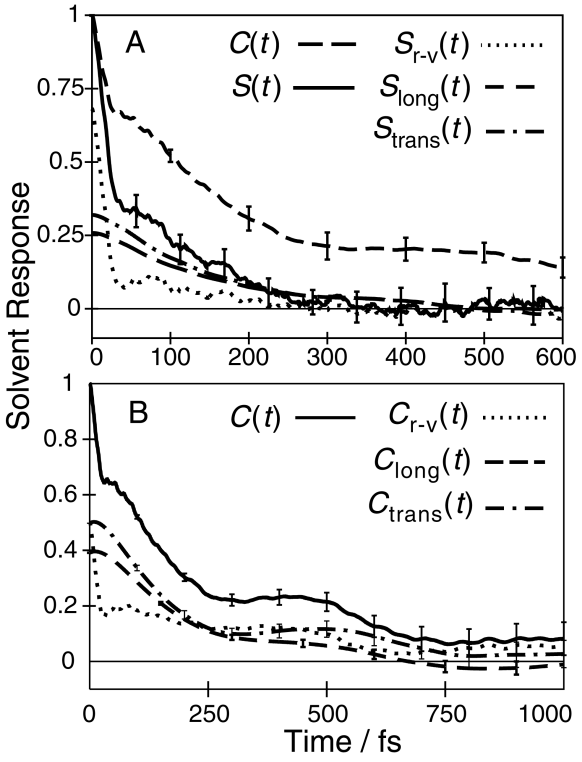

FIG. 1: A. Comparison between the total nonequilibrium, $S(t)$, and equilibrium, $C(t)$, solvent response functions, Eqs. 6 and 7, showing breakdown of LR. Integrated projections of the nonequilibrium solvent response onto various classical motions, Eq. 8, are also shown: S_{trans} is the contribution of all water com translations, S_{long} is the projection onto the longitudinal component of the water com translations (see text), and $S_{\text{r-v}}$ is the sum of the projections onto the water molecular vibrational and rotational motions. The normalization for all of the nonequilibrium curves show in Fig. 1A is $\overline{\Delta E}(0) - \overline{\Delta E}(\infty) = 1.47$ eV. B. The total equilibrium solvent response function, Eq. 7, and integrated projections of it onto different classical motions, Eq. 9; the subscripts used for each projection are the same as in panel A, except $C_{\text{r-v}}$, which represents the sum of the projections onto the water rotations, vibrations, and all of the cross-correlations. The error bars shown panels A and B are ±2 standard deviations [14].

* Electronic address: schwartz@chem.ucla.edu

[1] W. A. Steele. *Mol. Phys.*, 61(4):1031, 1987.
[2] B. M. Ladanyi and R. M. Stratt. *J. Phys. Chem. A*, 102:1068, 1998.
[3] M. J. Bedard-Hearn, R. E. Larsen, and B. J. Schwartz. *J. Phys. Chem. A*, 107(24):4667, 2003.
[4] M. J. Bedard-Hearn, R. E. Larsen, and B. J. Schwartz. *J. Phys. Chem. B*, 107:14464, 2003.
[5] B. J. Schwartz and P. J. Rossky. *J. Chem. Phys.*, 101:6902, 1994.
[6] M. Boero, M. Parrinello, K. Terakura, T. Ikeshoji, and C. C. Liew. *Phys. Rev. Lett.*, 90(226403-1), 2003.
[7] M. J. Bedard-Hearn. *Ph.D. thesis, UCLA*. 2006.
[8] For the equilibrium solvation correlation function, $\Delta E = \langle 1|\hat{H}|1\rangle - \langle 0|\hat{H}|0\rangle$, which is the energy gap between the ground ($|0\rangle$) and first excited ($|1\rangle$) states of the hydrated electron.
[9] R. E. Larsen, M. J. Bedard-Hearn, and B. J. Schwartz. *J. Phys. Chem.*, 2006. Submitted.
[10] K. Toukan and A. Rahman. *Phys. Rev. B*, 31:2643, 1985.
[11] P. J. Rossky and J. Schnitker. *J. Phys. Chem.*, 92:4277, 1988.
[12] M. J. Bedard-Hearn, R. E. Larsen, and B. J. Schwartz. *J. Chem. Phys.*, 123:234106, 2005.
[13] O. V. Prezhdo and P. J. Rossky. *J. Chem. Phys.*, 107:825, 1997.
[14] For more information, see http://www.aip.org/pubservs/epaps.html.
[15] D. Aherne, V. Tran, and B. J. Schwartz. *J. Phys. Chem. B*, 104(22):5382, 2000.